Rapid bioparticle concentration and detection by combining a discharge driven vortex with surface enhanced Raman scattering

Diana Hou, Siddharth Maheshwari, and Hsueh-Chia Chang[a)]
Department of Chemical and Biomolecular Engineering, Center for Microfluidics and Medical Diagnostics, University of Notre Dame, Notre Dame, Indiana 46556

(Received 10 November 2006; accepted 28 January 2007;
published online 16 February 2007)

Rapid concentration and detection of bacteria in integrated chips and microfluidic devices is needed for the advancement of lab-on-a-chip devices because current detection methods require high concentrations of bacteria which render them impractical. We present a new chip-scale rapid bacteria concentration technique combined with surface-enhanced Raman scattering (SERS) to enhance the detection of low bacteria count samples. This concentration technique relies on convection by a long-range converging vortex to concentrate the bacteria into a packed mound of 200 μm in diameter within 15 min. Concentration of bioparticle samples as low as 10^4 colony forming units (CFU)/ml are presented using batch volumes as large as 150 μl. Mixtures of silver nanoparticles with *Saccharomyces cerevisiae, Escherichia coli F-amp*, and *Bacillus subtilis* produce distinct and noticeably different Raman spectra, illustrating that this technique can be used as a detection and identification tool. © *2007 American Institute of Physics.*
[DOI: 10.1063/1.2710191]

INTRODUCTION

The analysis of pathogens viz. bacteria and viruses has proven to be difficult because of the low pathogen counts, $\sim 10^3$ colony forming units (CFU)/ml that is typically found in biological samples from living sources. Standard laboratory techniques would require the samples to be cultured to increase the concentration of bacteria by three orders of magnitude or more. This culturing step is a slow process that can consume anywhere from 24 h to weeks. The contribution of on-chip diagnostics to minimize the time needed for diagnosis is the removal of the bottleneck in time of sample culturing and instead to trap and concentrate the bacteria in the original sample to one location. Thus, the bacteria count at that location will be higher and can be seen with and without fluorescence.[1,2] Hence, by eliminating lab culturing steps, "Point-of-care" testing and other rapid diagnostics for malaria, environmental, and food borne pathogens can be developed for faster and portable detection methods.

Current on-chip concentration techniques employ electrokinetic methods, such as AC dielectrophoresis (DEP) and electrophoresis (EP) to manipulate and concentrate the bacteria.[3] DEP is the polarization of a particle in a nonuniform electric field, such that the particle will be attracted to regions of high field or low field, depending upon its polarizability relative to the medium.[4] The appeal of using DEP is its sensitivity to variations in size, shape, and conductivity of the particles. These particle characteristics can be used as a tool for separating different species, live and dead bacteria, and mixtures of bioparticles.[5] Moreover, this sensitivity can be tuned by varying the applied AC frequency and the conductivity of the solution to enhance or minimize the differences in the bioparticles that are being separated and concentrated.[6,7] However, the DEP force on the

[a)]Author to whom correspondence should be addressed. Electronic mail: hchang@nd.edu

 © 2007 American Institute of Physics

particle and the DEP velocity of the particle scale as a^3 and a^2, respectively, where a is the particle radius. Thus, in an applied field of 5 $V_{p\text{-}p}$ at 1 kHz, a 1 μm particle suspended in water has an average DEP velocity of ~ 1 μm/s. Therefore, particles on the order of 1 μm or smaller would only concentrate on an electrode by DEP when they are near the electrode surface. Alternatively, EP is the attraction of a charged particle to an opposing charged electrode. Unlike DEP, EP is not sensitive to size and shape of the particle, but is only dependent on the net charge of the particle. Thus, EP systems are not restricted by the particle size and can affect a larger percentage of particles in the bulk. However, strong DC fields are required to attract small particles to the electrodes in a short amount of time. This is a disadvantage for bacteria suspensions that are highly conductive, because it causes bubble generation and ionic gradients from the electrodes. These bubbles can block the flow in microchannels and the ion gradients can cause additional flow patterns, creating undesirable and unreliable results in a microchip.

An alternative method for concentrating bacteria is to couple DEP with an AC electro-osmotic (ACEO) flow.[7,8] It has been shown that when an AC field is applied across a parallel planar electrode system, the ACEO flow will generate vortices above the electrode surfaces and form a converging flow stagnation point on the electrode surface.[1,9] As the particles are swept from the bulk towards the electrode, the DEP force on the electrode attracts the particles to the electrode surface where they are rapidly concentrated. However, because the driving mechanism of the vortices is restricted to the electrode surface, the vortices can only extend a few hundred microns above the electrodes.[1] Thus, using vortices generated by the induced ACEO flow on the electrodes can only affect a small portion of the liquid sample and is unable to handle larger volumes. In this paper, we demonstrate the use of a novel converging flow, that instead of depending upon short-range electrokinetic effects, works via a long-range converging flow that is not localized to submerged-fabricated electrodes, but is generated by momentum transfer on the free liquid surface.

Upon concentration of the bacteria, detection methods and other diagnostics can be employed on the concentrated region. Current on-chip detection methods include micro-PCR, impedance, immunocolloids, and antibody tagging.[10] These methods are specific in determining different properties of the sample in terms of detection. For example, PCR is very specific in identifying the strain of the bacteria because the method is based on the nucleic material. However, PCR cannot be used to detect the quantity or the viability of the bacteria because they are killed in the process of DNA extraction. Furthermore, impedance can determine the relative quantity and viability of the bacteria because the resistivity across bacteria differs when it is alive or dead. However, it cannot identify the strain of the bacteria. Immunocolloids functionalized with antibodies are also specific in identifying the bacteria, but the colloids with and without bacteria must be sorted prior to detection. Though most of these methods can be used to rapidly identify bacteria in microdevices, they require specific sample preparation, washing, and separation steps that create additional problems for chip-scale separations.

An on-chip detection technique that can identify the concentrated bacteria in a sample with minimal or no sample preparation would be ideal for microchip and rapid diagnostics. A detection technique that can perform on-chip detection is spectroscopy, such as infrared (IR), ultraviolet and visible (UV-Vis), and Raman. Recently these techniques have been implemented as on-chip detection methods because of their sensitivity to complex structures and molecular differences in bacteria, bioparticles, DNA, and chemical compounds.[11] Raman and IR spectroscopy both measure the vibrating, bending, and stretching modes of the bonds of the molecules, hence making these spectra sensitive to different molecular structures.[12] Spectroscopy has been applied to characterize bioparticles, using the different proteins, amino acids and sugars found on the surface of the bacteria. In fact, there has been Raman spectroscopic identification of single cells, DNA, live and dead bacteria, and tumor and nontumor cells.[13–15] While Raman and IR are similar in their measurements, they differ in that IR measures the absorption effect during the vibrational modes and can only detect the vibration that results in a dipole change. Alternatively, Raman measures the scattering effect and can only detect changes in the polarization of the molecule. This scattering makes the Raman spectrum very specific to the bioparticle being identified, creating a "fin-

gerprint" of the bioparticle.[16] This "fingerprint" of bacteria, DNA, and bio-materials has led to the recent interest in using Raman spectroscopy for detection. However, Raman scattering is a weak scattering effect, roughly only 1 in 10^6 photons that scatter results in a Raman scatter. Thus, the bioparticles must be present in very high concentrations to obtain a definitive spectrum or the scanning time must be increased to reach sufficient Raman scattering. The fastest reported time for bacteria detection with Raman spectroscopy is 6 h, where no preconcentration was performed and considerable culturing of the bacteria was used.[17]

With the addition of metal nanoparticles to the bioparticles suspension, the scattering efficiency can be enhanced up to a factor of 10^6. However, these metal nanoparticles must be chemically bonded, adsorbed on the surface of, or be in close proximity to the bioparticles such that its electron cloud will interact with the bioparticle's electrons. The metal nanoparticles will enhance the polarizability of the bioparticle, thus increasing the Raman scattering and intensity of the Raman shifts.[18] This enhanced Raman scattering with metal nanoparticles, surface-enhanced Raman scattering (SERS), is currently being investigated for the rapid detection of bacteria in realistic sample concentrations. Using SERS, lower concentration limits have been shown to be able to identify complex structures and differentiate species in bacteria, chemical agents, and nucleic material.[16,19] A scanning time of only 20 s has been reported for the rapid detection of bacteria using SERS, however, the concentration of bacteria used was directly from a growth plate ($\sim 10^9$ CFU/ml).[20]

Another difficulty in detecting bacteria with spectroscopy is that the bacteria needs to be immobilized, either in the suspension or on a substrate. This process can be accomplished using optical tweezers to eliminate Brownian motion away from the beam during scanning. However, optical tweezers can be detrimental to the bacteria if focused on the bacteria for long periods of time.[15] Though concentration limits are lowered with SERS, it is still too high for on-chip diagnostics and needs to be coupled with a preconcentration method prior to using SERS to identify a sample. To our knowledge, the coupling of Raman spectroscopy with a preconcentration microfluidic method has not published in literature as of yet.

In this article, we present a novel coupling of a preconcentration method with SERS to rapidly concentrate and detect low bioparticle count samples. The concentration of bacteria to one location enhanced the detection of the Raman scattering by increasing the location concentration that is being processed. On-chip detection using SERS can be performed on the concentrated location with no additional sample preparation. A 150 μl sample is shown to be concentrated using a discharge driven vortex to convect the particles to a converging flow stagnation point where gravitational forces or separate Coulombic forces prevent the particles from resuspending. Within 15 min, the concentration vortex yields a packed mound with a width of ~ 200 μm. Latex particles, *Saccharomyces cerevisiae, Escherichia coli*, and *Bacillus subtilis* were concentrated using this vortex and detected using Raman spectroscopy. Adding silver nanoparticles to the bioparticle suspensions produced distinctly enhanced and different signals for the three types of bioparticles. Concentrations as low as 10^4 CFU/ml were detectable using the discharge driven vortex to preconcentrate the bioparticles, creating a locally high concentration of bioparticles. A secondary electrode configuration was developed to couple electrophoretic effects with the hydrodynamic flow to enhance the trapping efficiency of submicron bioparticles and to immobilize bioparticles onto an electrode surface.

THEORY

Ionic wind generation

Charge buildup on a sharp tip electrode under a high frequency AC field ($\sim$20–180 kHz) can create a stream of ions away from the tip towards a ground electrode. This stream of ions, an ionic wind, is generated at the tip due to its sharpness and corona discharge effects.[21,22] As the ions are propelled from this sharp electrode, they collide with air molecules which in turn collide with the liquid surface, thus imparting their momentum onto the liquid interface. A continuous stream of ions from the electrode tip acts as a point source of momentum on the liquid interface, driving an

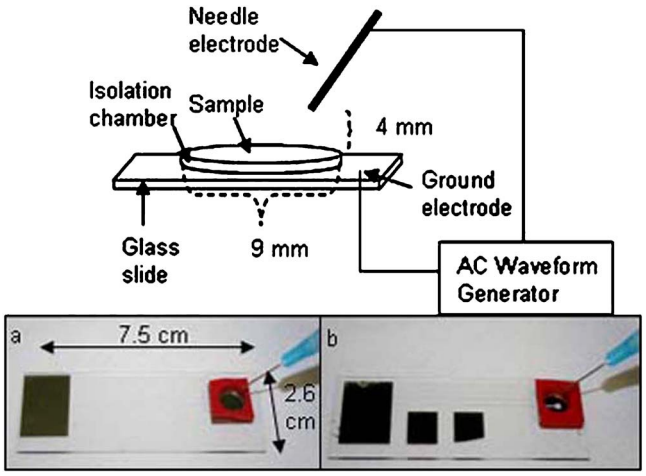

FIG. 1. Schematic of the experimental set-up: A sharp tip needle electrode is connected to an AC waveform generator and a ground electrode on the glass slide. The needle is suspended 4 mm above a liquid sample that is held in a chamber that is 9 mm in diameter and 2.5 mm deep. (a) An image of the glass slide with a square electrode as the ground electrode. (b) An image of the glass slide with secondary electrodes fabricated at the center of the ground electrode.

interfacial flow. With the liquid being confined by solid boundaries, vortices are generated on the surface. It has been shown that the size, shape, direction of rotation, and angular velocity is dictated by the placement of the sharp electrode with respect to the liquid surface and the magnitude of the applied field.[21] With the electrode placed at the center, a symmetric system of equal sized vortices is produced, while an off-center placement makes one of the vortices dominant. For our purposes, a single dominating vortex is desired and consequently the sharp electrode is placed near the corner of the liquid bulk and suspended ~4 mm above the liquid surface. The electrode configuration is shown in the schematic in Fig. 1(a). The electrode at the bottom of the reservoir is a square electrode that covers the entire reservoir bottom and acts as a ground for the system. It should be noted that the sharp tip, which is the working electrode is not in contact with the liquid sample, which is a distinct advantage.

Flow field

The interfacial vortex driven by the ionic wind generates a bulk flow in the reservoir that is similar to the classical spiral flow below a rotating disk.[23] When inertia can be neglected, then the liquid flow mirrors the motion of the rotating plate and an azimuthal vortex is produced. At creeping flow conditions with the equations and boundary conditions being linear, the spatial symmetry of the boundary conditions is preserved,[24] with velocity at any axial position directly proportional to its angular velocity and its relative height, which is the ratio of the axial distance from the bottom substrate to the height of the liquid chamber. The second proportionality is due to no-slip at the bottom substrate and maximum velocity on the rotating surface. Consequently, the axial and radial velocities are identically zero everywhere in the domain and the flow field is azimuthal. At higher Reynolds numbers, ~10, a secondary inertial flow is generated, which is directed radially outwards at the surface of the liquid due to a centrifugal force and radially inwards at the bottom due to flow continuity. At the center of the vortex on the bottom of the reservoir, the liquid is pushed upward again and the entire cycle is repeated. The combination of these two flow fields' results in a spiral or a torrodial flow field, depending upon the actual magnitude of the secondary flow with respect to the primary flow, through the entire bulk, as sketched in Fig. 2(a), and a converging flow stagnation point on the bottom of the chamber, as depicted in Fig. 2(b). Particles present in the liquid bulk will be convected by the flow and follow the fluid streamlines, especially on the free liquid surface. Near the stagnation point, however, the fluid velocity is reduced due to a no-slip condition on the stationary substrate. Depending upon the

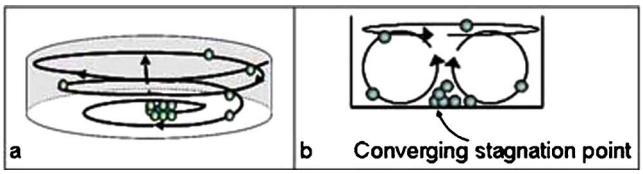

FIG. 2. Discharge driven vortex: (a) Vortex through the entire liquid convects the particles throughout the bulk to one location. (b) The side view of the chamber showing the primary interfacial flow and the secondary inertial flow. The secondary torrodial flow creates a converging stagnation point at the bottom of the chamber that when combined with gravitational forces and Coulombic, can trap particles there.

relative magnitude of the sedimentation force as well as the hydrodynamic force on the particle, the particles can either be drawn to the substrate by gravity, or be resuspended into the bulk. Thus, this converging flow field coupled with a particle body force, gravity in this case, creates a particle trap at the stagnation point. This flow field has been shown to be able to separate red blood cells from the plasma in blood samples as a microfluidic blood separator.[25] As the convection velocity exceeds 1 cm/s, the trapping is rapid. Hence, this far-reaching microflow significantly extends the domain of attraction of short-range DEP traps. Since sedimentation is clearly contingent upon the volume and density of the particle, there is a critical limit to the size and density of the particle that can be trapped that is dependent upon the liquid velocity. Smaller particles are less affected by gravity and are more likely to resuspend at higher velocities. Additionally, larger particles will settle faster than the circulation time of the inertial flow and the particles will settle to the bottom of the chamber, but will not be convected to the stagnation region. Therefore, there is an optimum velocity profile for trapping depending upon the particle dimensions and specific gravity. Given the small size of most bacteria, resuspension is a problem. Additionally, since the bacteria are negatively charged, there is significant Coulombic repulsion among them, which makes aggregation difficult. Consequently, additional body forces on the bacteria are needed to augment gravitational sedimentation and prevent resuspension.

Spiral electrode

To aid in the immobilization of the bacteria on the electrode substrate an additional spiral electrode was fabricated at the predetermined concentration location. When a small DC bias is applied through the electrode, roughly 3 V, the particles, which are slightly negatively charged are attracted to the postively charged electrode. This additional force on the particles in the z-direction at the stagnation point increases the net body force on the particles in the suspensions, allowing for micron and submicron particles to be trapped on the electrodes as well as increases the quantity of particles that can be trapped. In addition to extenting the criteria for the size of the particle that can be trapped, the particles were immobilized onto a gold electrode surface, increasing the Raman signal.

EXPERIMENTAL SECTION

Materials

A 35 nm electrode (5 nm Ti/30 nm Au) was fabricated by electron beam lithography on a surface treated glass slide using standard lithography techniques. Two designs were used, a square and a spiral electrode. The square electrodes were fabricated with dimensions of a 1.3 cm by 1.3 cm^2, while the spiral electrode measured 110 μm wide with a 10 μm electrode 10 μm gap spiral and was surrounded by the ground electrode, as seen in Fig. 9. All the electrodes were connected to contact pads on the opposite end of the glass slides. Isolation reservoirs (Grace Biolabs, USA) measuring 9 mm in diameter and 2.5 mm deep were aligned on the glass slide with an adhesive coating on one side which was used to adhere the well onto the electrode/glass surface. When the liquid was filled in the well, the top surface of the liquid remained a free surface. A sharp tip syringe needle was used as the live electrode and both the needle and the

ground electrode were connected to a high voltage transformer. The needle was suspended ~4 mm above the sample so that the needle was not in contact with the liquid. Although a large sized power source during the development of this technique was used for precise generation of the electric signals needed, the power supply can be miniaturized to a hand-held generator. The sinusoidal AC signal was generated by a function/arbitrary waveform generator (Agilent 33220A) and magnified through a RF amplifier (Powertron 250 A, 10 Hz–1 MHz) and a secondary high voltage transformer (Industrial Test Equipment, 10 kHz–70 kHz). The output was measured through high voltage probes (Tektornix, P6015A) connected to an oscilloscope. The device was imaged using an Olympus 1×71 microscope and an I-speed CDU camera system (Olympus America). A variable DC field was applied using an universal AC adapter (RCA AH5WH) that can output DC voltages ranging from 1.5–12 V-DC.

Particle suspensions comprised of 1 μm and 5 μm latex particles (Fluka, Sigma-Aldrich, USA) were suspended in deionized (DI) water (Millipore) in concentrations ranging from 10^4–10^7 particles/ml. *S. cerevisiae*, commonly known as baker's yeast (Fleischmann), was revived in a solution of warm water and sugar for 15 min. The suspension was then diluted in water to reach concentrations of 10^4–10^6 CFU/ml. *S. cerevisiae*, though nonpathogenic, is typically used as a model eukaryotic cell because of its relatively fast and simple growth process. It is also ideal for these experiments because it provides a large difference in bioparticle size, shape, and cell wall composition in comparison with the bacteria: 5 μm versus 1 μm, spherical versus rod-shaped, and eukaryotic cell wall versus prokaryotic cell wall. *E. coli* (ATCC 700891) and *B. subtilis* were grown overnight in tryptic soy broth at a temperature of 37 °C. The suspensions were washed and resuspended in saline to reach a concentration of 10^7 CFU/ml. Both of these bacteria are rod-shaped with an aspect ratio of 1:0.5 μm. Both *E. coli* and *B. subtilis* are used as model bacteria for most prokaryotic experiments. However, the main difference between the two types is that *E. coli* is a gram negative bacterium while *B. subtilis* is a gram positive bacterium. Thus *E. coli* has additional lipids and polysaccharides on the outer membrane of its cell wall while *B. subtilis* has a thick peptidoglycan wall.

Silver nanoparticles were synthesized by the method described by Lee and Meisel[26] at concentrations of 4 mM, with a diameter of roughly 80 nm. A Renishaw 2000 Raman microscope was used for all Raman analysis with a 514.5 nm laser for optimal surface-enhanced Raman scattering with the silver nanoparticles. The laser power was recorded at 15 mW for all experiments except for the *B. subtilis*, which had a lower intensity of 12 mW due to extended laser usage. After concentration, all samples were scanned under a 20× objective.

Methods

As shown in Fig. 1, the needle was suspended above the liquid surface at an angle of 45° and placed offset from the center of the reservoir in order to generate one large surface driven vortex. The particle suspensions were placed in the reservoir and subjected to a high frequency AC field for 15 min at a constant frequency of 40 kHz with a voltage ranging between 3 and 5 kV. The Raman microscope was then focused onto the packed mound and scanned for an extended spectrum for 30 s with 1 accumulation. For surface-enhanced Raman scattering, the bioparticle suspensions were mixed with the silver nanoparticles in a volumetric ratio of 3:1 μL to reach a net volume of 160 μL. The new suspension was then subjected to the same high frequency AC field for 15 min and scanned under similar conditions with the Raman microscope. Data capture and instrumentation control for the Raman microscope was carried out via the GRAMS software. The ASCII data was exported into Excel and MATLab for further data analysis.

RESULTS AND DISCUSSION

Latex particles

Using the square electrodes, a 150 μL suspension of 5 μm latex particles at a concentration of 10^6 particles/ml was concentrated under an applied field of 3 $kV_{p\text{-}p}$ with a frequency of 40 kHz. A vortex encompassed the entire sample and immediately began to bring the particles to

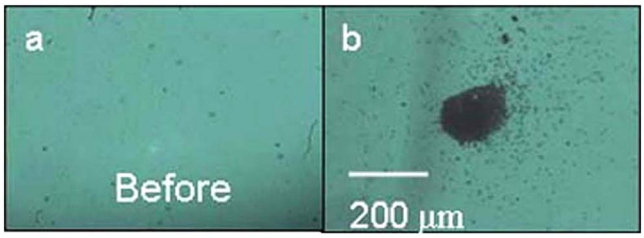

FIG. 3. Concentration of 5 μm latex particles by the discharge driven vortex. Images are a bottom view of the sample, through the glass slide. (a) Prior to application of the applied field of 3 kV, 40 kHz, the stagnation point is relatively clear of latex particles. (b) Concentration of the latex particles 15 min after the AC field is applied. A packed mound of particles is apparent and is concentrated to a region that is roughly 200 μm in diameter.

the stagnation point at the bottom of the reservoir. To contrast the effect of the packed mound, an image was taken prior to the application of the field, shown in Fig. 3(a), while Fig. 3(b) was taken after a time lapse of 15 min of concentration. The mound of particles measured is ~200 μm in diameter and it is clear that the particles not only concentrated to a small region in the x-y plane but also concentrated in the z-direction creating a three-dimensional mound. A suspension of ($\sim 10^4$ particles/ml), was concentrated under similar electric field strengths and the concentrated mound measured to be roughly 100 μm in diameter. A higher voltage was applied at a lower frequency, 3.72 $kV_{p\text{-}p}$, 20 kHz, to reach higher velocities within the vortex. The image of the particles trapping at the stagnation point is shown in Fig. 4 with a time lapse of 2 min between each image. As can be seen in the images and the corresponding histogram of the trapping region as a function of time, a significant amount of particles were trapped at the stagnation region within 4 min of the applied field. After 12 min of trapping, the concentration of the packed mound continued to increase until it reached a maximum.

From the histogram it is clear that as the particles were concentrating, they were not expanding the trapping radius. This is most likely attributed to the high velocity of the vortex that continually swept the particles from the bulk towards the stagnation point instead of rolling the particles towards the stagnation region. The sedimentation force is proportional to the density difference between the particles, the media, and the particle volume. Since the density difference does not significantly vary for the particles and bacteria considered in this work, it is the length scale that determines the large particle size, the sedimentation velocity is much greater than the circulation velocity of the vortex and the particles settled to the bottom of the chamber. Once they had settled, the only way for the particles to trap at the stagnation point is for them to roll along the bottom of the reservoir towards the stagnation point. Therefore, at the stagnation point, the particles do not form a packed mound and instead form a monolayer of particles extending in the x-y plane. At very small particles sizes, the sedimentation velocity is much smaller than the circulation velocity and the particles are continually resuspended and no trapping occurred. Hence,

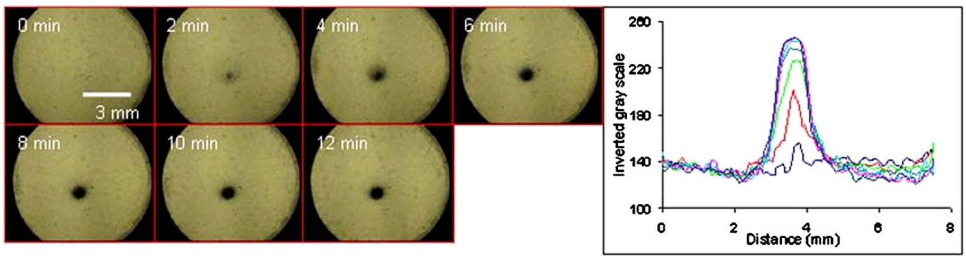

FIG. 4. Time lapse imaging of the concentration of 5 μm latex particles under a field of 3.96 kV and 20 kHz. The images are taken 2 min apart; trapping at the stagnation point is apparent within 2 min of applying the field. Further concentration in the z-axis is shown as the packed mound becomes darker but the width of the regions remains the same. The histogram across the packed mound is taken at 2 min intervals and is seen to reach a maximum in the packing with 10 min.

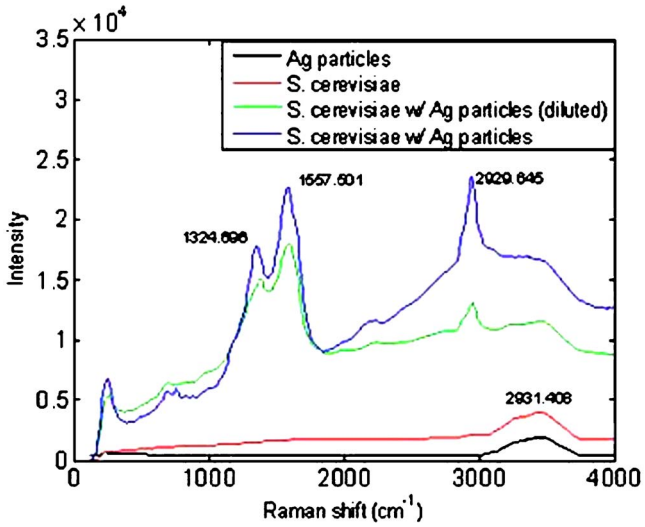

FIG. 5. Raman spectra of the concentrated *S. cerevisiae* under a field of 3.96 kV and 40 kHz for 15 min: The black line represents the silver nanoparticles added to the bioparticle suspension and shows no additional peaks contributing to the spectrum. The red line represents a sample of *S. cerevisiae* alone and indicates the spectrum is weak and most peaks are indistinguishable. A mixture of *S. cerevisiae*, at a concentration of 10^5 CFU/ml, and silver nanoparticles were concentrated and their spectrum is shown by the blue line, where distinguishable peaks are seen. A dilute suspension of *S. cerevisiae* (10^4 CFU/ml) and silver nanoparticles is depicted by the green line, which also shows characteristic peaks, but at a lower intensity than the previous sample.

for a small packed mound to form, the particle sedimentation velocity must be slightly greater than that of the circulation and resuspension velocity so that when the particles are trapped at the stagnation point they are convected to the stagnation region from the bulk.

The packed mound was then analyzed using Raman spectroscopy. The Raman spectrum of the latex particles is well characterized and can be found on the vendor's website. From the acquired Raman signal, significant peaks were found at 3058.7 cm^{-1} and 1002.4 cm^{-1} which are comparable to the peaks found in literature, verifying that the Raman shift can be detected on the concentrated mound.

S. cerevisiae concentration and detection

Mixtures of *S. cerevisiae* and nanoparticles were concentrated under similar conditions and scanned for their Raman shifts. The spectra for the mixtures, along with a pure *S. cerevisiae* suspension and a pure nanoparticle suspension are presented in Fig. 5. The first spectrum taken with silver nanoparticles only produced a weak signal, as depicted by the black line in Fig. 5, indicating that the nanoparticles did not introduce any additional peaks in the spectrum. A spectrum of a pure *S. cerevisiae* suspension of 10^6 CFU/ml which was then concentrated using the spiral trap also produced a weak signal as depicted by the red line in Fig. 5. The characteristic peaks that are found in literature for *S. cerevisiae* were not prevalent.[13] Thus, Raman scattering alone cannot produce a distinct signal in the short scanning time of the concentrated packed mound.

Mixtures of silver nanoparticles and *S. cerevisiae* (10^5 CFU/ml) were then concentrated and scanned. A strong signal was produced, as depicted by the blue line in Fig. 5, with distinct peaks that correspond to those found in the literature. A lower concentration of *S. cerevisiae* 10^4 CFU/ml, mixed with 20 μL of nanoparticles was also probed and found to produce strong signals, as seen by the green line in Fig. 5, though of slightly less intensity than that of the previously mentioned mixture. The decrease in intensity between the two concentrations is not necessarily a linear relationship to the concentration of the sample. It is highly dependent on the concentration within the size of the beam. Though the concentration region is roughly 200 μm,

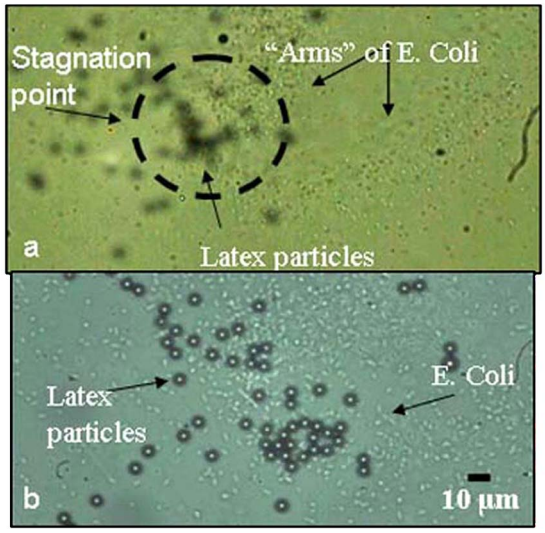

FIG. 6. Stagnation point with 5 μm latex particles and *E. coli* (10^7 CFU/ml). (a) *E. coli* spiraling towards the stagnation point, forming the "arms" of the spiral. (b) At the stagnation point, the 5 μm latex particles and the *E. coli* are concentrated in the same spot, indicating the location of concentration is not size dependent. The *E. coli* also do not form the packed aggregates and the packed mound, instead expanding the concentration region in the *x-y* plane.

the concentration of bioparticles is not necessarily uniform across the entire region that is sampled with the beam size, roughly 50 μm. Therefore, using Raman spectroscopy to quantify the concentration of bioparticles within the trapping region requires further calibration using different quantification techniques viz. cytometry, which was not examined in this work. Though SERS enhancement has been reported to reach orders of magnitude in the scattering enhancement, the experimental results shown are roughly only an order of magnitude in terms of intensity enhancement of the spectra. This lower enhancement level may be caused by an insufficient addition of nanoparticles such that not all the particles were able enhance the cells polarizability. However, as seen in Fig. 5, even with the small quantity of nanoparticles that were added to the *S. cerevisiae* suspension, an order of magnitude of enhancement was detectable in the packed mound.

E. coli concentration and detection

Similar conditions as the *S. cerevisiae* were used to concentrate the *E. coli* at the stagnation point. Under an applied field of 3.96 kV_{p-p}, 40 kHz, a sample of 10^7 CFU/ml of *E. coli* was concentrated to an area of roughly 300 μm wide. As can be seen in Fig. 6, the *E. coli* were concentrated to a specific area, but the width of the concentrated area is much larger than that of the *S. cerevisiae* or the latex particles. Also, unlike the two previous experiments, the *E. coli* were reluctant to form a three-dimensional packed mound and only concentrated by extending out in the *x-y* plane. This might be due to the negative surface charge of the bacteria thus preventing them from aggregating. Due to their small size, roughly 1 μm, in comparison to the latex particles and the *S. cerevisiae*, roughly 5 μm, the body forces in attracting the *E. coli* to the electrode surface are much weaker, and are more subjective to the hydrodynamic recirculation; thus exemplifying that a critical angular velocity exists for the size of the bioparticles that can be trapped by pure gravitational forces. This occurs because if the angular velocity is too high, all the particles will be resuspended due to strong recirculation forces. Thus, there exists an optimal velocity range where trapping is maximized.

The local bacteria count at the stagnation point is still high and restricted to a small region on the gold electrode. Though this concentration is not as pronounced as with the larger bioparticles, the vortex through the sample is strong enough to convect the bacteria to the stagnation region and the gravitational force on the *E. coli* is large enough to prevent them from resuspending.

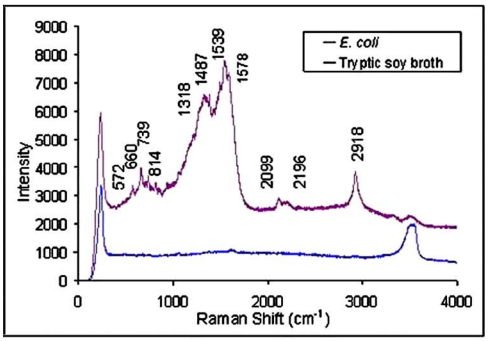

Shift (cm^{-1})	Corresponding bonds
572	C-Cl, C-Br, C-I, C=S
660	C-Cl, C-Br, C-S aliphatic,
739	C-Cl, C-F, C-S,
814	C-O-C ethers,
1318	Carboxylate salt, Nitro
1487	Aromatic ring,
1539	Nitro, Aliphatic azos
1587	Aromatic/hetero ring, Nitro, Amide
2099	Isothiocyanate
2196	Alkyne
2918	-OH, C-CH$_3$

FIG. 7. Raman spectra of the *E. coli* experiments: The purple line indicates the concentrated *E. coli* ($\sim 10^7$ CFU/ml) under an applied field of 3.96 kV and 40 kHz for 15 min. Additionally, the growth media, tryptic soy broth is shown by the blue line to indicate that no additional peaks were contributing to the bacteria spectrum. A table of typical corresponding bonds found at the listed peaks that are typically found in literature, is shown adjacent to the spectrum.

A Raman spectrum was taken of the concentrated stagnation region as depicted by the purple line in Fig. 7. An additional spectrum was taken of the growth media, tryptic soy broth, to ensure that the sample was thoroughly washed and any remnants from the broth were not contaminating the *E. coli* spectrum, as seen by the blue line in Fig. 7. Due to the various proteins and molecules present on the *E. coli*'s surface, the peaks can represent various bonds from the complex molecules. The peaks listed for the *E. coli* spectrum and possible molecular structures that are commonly present as peaks in those regions are shown in the adjoining table in Fig. 7.[12] It indicates the presence of a variety of organic and inorganic bonds, as is expected from a living organism.

B. subtilis concentration and detection

B. subtilis ($\sim 10^7$ CFU/ml) was concentrated in a mixture of silver nanoparticles under the same applied AC field and ratio of nanoparticles to bacteria. The Raman spectrum taken of the *B. subtilis* produced less definitive peaks than the *E. coli* spectrum, possibly due to the decrease in the laser power intensity from 15 mW to 12 mW. However, observable peaks were still present to indicate differences in the spectrum when compared with the other bioparticles. In Fig. 8, the three spectra corresponding to the *S. cerevisiae*, *E. coli*, and *B. subtilis* are shown with adjusted intensities to emphasize the differences in their Raman shifts. These differences in their peaks

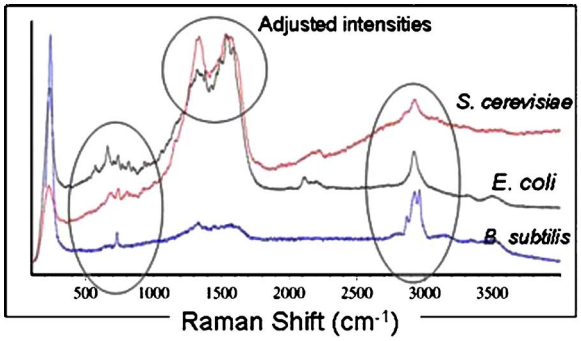

FIG. 8. Combined spectra of *S. cerevisiae*, *E. coli*, and *B. subtilis* with their intensities adjusted to emphasize the differences in the spectra. Regions between 500 and 1000 cm^{-1} tend to hold the most characteristic peaks and can be seen to differ between the three spectra. The broad peak at 1500 cm^{-1} is apparent in both the *S. cerevisiae* and the *E. coli* spectra, however, the peaks on the top of this broad peak are different.

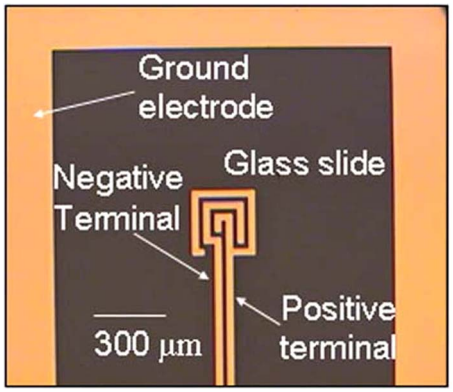

FIG. 9. Image of the secondary spiral electrode fabricated on the glass slide with the ground electrode. A 3 V-DC field is applied between the two electrodes in the spiral to electrophoretically attract bioparticles and aid in their trapping and immobilization.

are comparably different and can be used as a way to differentiate between the three different bioparticles.

Spiral electrode

In order to lower the trapping criteria and enhance the trapping of submicron particles, additional electrodes were fabricated on the glass substrate in addition to the ground electrodes, as seen in Fig. 9. With an additional applied field, the submicron bioparticles can be attracted to, and immobilized on the gold electrodes, not only enhancing the quantity that is trapped but also eliminating Brownian motion effects that are otherwise prevalent for the smaller particles. A 1 μm latex particle suspension in DI water at a concentration of 10^5 particles/ml was placed in the reservoir and concentrated under an applied field of 3.96 $kV_{p\text{-}p}$ and 40 kHz. Though the spiral electrodes were not connected, the 1 μm particles still concentrated on an electrode surface, as seen in Fig. 10(a). The center of the spiral was placed near, but not directly on the electrodes, so as the particles were convected near the electrodes, they were attracted to the electrode surface. The induced polarization effect of the electrodes is attributed to the low conductivity of the medium ($\sim$18 μS/cm). A field gradient is generated in the bulk, polarizing the electrodes such that the particles will be attracted to one electrode. In contrast, for particles suspended in a highly conductive solution, such as saline, no field gradient exists and the electrodes cannot be polarized.

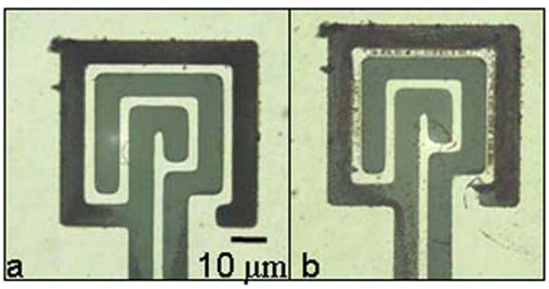

FIG. 10. Polarization of the spiral electrode due to the field gradients. (a) A field applied to a 1 μm latex particle suspension where the spiral electrodes are not connected to any power supply. Due to the low conductivity of the solution, the electrodes become polarized and attract the particles to the electrode surface. (b) Upon removal of the applied AC field, a small 3 V-DC is applied across the two electrodes. The particles are immobilized on the electrode surface and nearby particles are attracted to the electrode.

The same experiment was repeated with the 1 μm latex particles suspended in saline and the spiral flow was formed but no particles were attracted to the electrodes due to pure field gradient effects.

In the DI water experiments, upon removal of the AC field, the particles began to diffuse away from the electrode. Therefore, an additional field was applied to the spiral electrodes. If an AC field was applied, DEP forces would cause the particles to trap at the electrode edges and effects such as ACEO flow would cause the particles to resuspend. In contrast, under a DC field, the particles would be attracted and immobilized on only one electrode, which is already occurring due to the polarization. Thus, upon the concentration of the particles to the polarized electrode, a 3 V-DC field was applied to the secondary electrodes using the RCA universal AC adapter and connected such that the outer electrode of the spiral was connected to the positive terminal and the inner spiral to the negative terminal of the adapter. Because the latex particles have a slight negative charge, the positive terminal is desired for the outer electrodes since the particles are already attracted and located near this electrode. Upon connection of the adapter, the particles became trapped to the entire electrode surface and nearby particles can be seen being attracted to the positively charged electrode, as seen in Fig. 10(b). When the terminals were switched, the particles were attracted to the opposite electrode, thus confirming that the particles attractive force is due to the electrophoretic attraction between the particle and the electrode. This secondary electrode increased the trapping efficiency of micron and submicron particles and immobilized these particles to the electrode surface, eliminating effects due to Brownian motion and like charge repulsion effects.

CONCLUSION

Using a discharge driven vortex, we have been able to concentrate 150 μl bioparticle samples with a concentration as low as 10^4 CFU/ml within 15 min and obtain characteristic Raman spectra using silver nanoparticles. We were able to create a locally high concentration of bioparticles from a dilute sample and then proceeded to detect and identify the sample using surface-enhanced Raman scattering. Typical Raman spectroscopy requires high concentrations of their analyte, around 10^9 units/ml. We have used a sample of 10^4 CFU/ml and were still able to obtain a characteristic spectrum within 15 min showing the advantage of preconcentration with the vortex flow. Further developmental work towards creating a more portable chip-size detection system using the discharge driven vortex and Raman spectroscopy include substituting the AC wave-form generator with a hand-held generator and designing fiber optics that are capable of detecting the Raman scatter for on-chip analysis.[27] This is presently being carried out.

ACKNOWLEDGMENTS

The authors would like to thank Dr. G.N.R. Tripathi and Bert Ji of the Notre Dame Radiation Laboratory for their Raman microscope and providing the silver nanoparticle suspensions. The authors also thank Dr. Shramik Sengupta for culturing the bacteria samples and Dr. Eugene Chang of the University of Chicago Medical School for supplying the *B. subtilis*. Diana Hou is partially funded through the Bayer Predoctoral Fellowship, Siddharth Maheshwari is partially funded through the Center of Applied Mathematics and all authors are supported by Grant Nos. NSF CT504-54956, NASA NAG3-2701, and NASA NAG5-10503.

[1] K. F. Hoettges, M. P. Hughes, A. Cotton, N. A. E. Hopkins, and M. B. McDonnell, IEEE Eng. Med. Biol. Mag. **22**, 68 (2003).
[2] J. Wu, Y. Ben, D. Battigelli, and H.-C. Chang, Indust. Eng. Chem. Res. **44**, 2815 (2005).
[3] J. Voldman, Annu. Rev. Biomed. Eng. **8**, 425 (2006).
[4] H. A. Pohl, *Dielectrophoresis* (Cambridge University Press, London, Great Britain, 1978).
[5] H. Li and R. Bashir, Sens. Actuators B **86**, 215 (2002); Il Doh and Y.-H. Cho, Sens. Actuators, A **121**, 59 (2005).
[6] W. M Arnold, IEEE Trans. Appl. Ind. **37**, 1468 (2001).
[7] Z. Gagnon and H.-C. Chang, Electrophoresis **26**, 3725 (2005).
[8] N. G. Green, A. Ramos, A. Gonzalez, H. Morgan, and A. Castellanos, Phys. Rev. E **61**, 4011 (2000); M. P. Hughes, Nanotechnology **11**, 124 (2000).
[9] J. Wu, Y. Ben, and H.-C. Chang, Microfluid and Nanofluid **1**, 161 (2005).

[10] J. Suehiro, A. Ohtsubo, T. Hatano, and M. Hara, Sens. Actuators B **119**, 319 (2006); A. Bange, H. B. Halsall, and W. R. Heineman, Biosense. Bioelectron **20**, 2488 (2005); K. Cheung, S. Gawad, and P. Renaud, Cytometry Part A **65A**, 124 (2005); I. V. Kourkin, M. Ristic-Petrovic, E. Davis, C. G. Ruffolo, A. Kapsalis, and A. E. Barron, Electrophoresis **24**, 655 (2003); M. G. Roper, C. J. Easley, and J. P. Landers, Anal. Chem. **77**, 3887 (2005).
[11] T. Vo-Dinh, F. Yan, and M. B. Wabuyele, J. Raman Spectrosc. **36**, 640 (2005); M. Kummerle, S. Scherer, and H. Seiler, Appl. Environ. Microbiol. **64**, 2207 (1998).
[12] E. Smith, and G. Dent, *Modern Raman Spectroscopy: A Practical Approach* (John Wiley & Sons, 2005).
[13] P. Rosch, M. Harz, M. Schmitt, and J. Popp, J. Raman Spectrosc. **36**, 377 (2005).
[14] G. J. Thomas, Jr., Annu. Rev. Biophys. Biomol. Struct. **28**, 1 (1999); B. W. D. de Jong, T. C. Bakker Schut, K. Maquelin, T. vander Kwast, C. H. Bangma, D.-J. Kok, and G. J. Puppels, Anal. Chem. **78**, 7761 (2006); Y. C. Cao, R. Jin, and C. A. Mirkin, Science **297**, 1536 (2002).
[15] C. Xie, C. Goodman, M. A. Dinno, and Y.-Q. Li, Opt. Express **12**, 6208 (2004).
[16] R. M. Jarvis and R. Goodacre, Anal. Chem. **76**, 40 (2004).
[17] K. Maquelin, L.-P. Choo-Smith, H. P. Endtz, H. A. Bruining, and G. J. Puppels, J. Clin. Microbiol. **40**, 594 (2002).
[18] K. Kneipp, H. Kneipp, I. Itzkan, R. R. Dasari, and M. S. Feld, J. Phys.: Condens. Matter **14**, R597 (2002).
[19] F. Yan, M. B. Wabuyele, G. D. Griffin, A. A. Vass, and T. Vo-Dinh, IEEE Sens. J. **5**, 665 (2005); T. Vo-Dinh, D. L. Stokes, G. D. Griffin, M. Volkan, U. J. Kim, and M. I. Simon, J. Raman Spectrosc. **30**, 785 (1999); W. R. Premasiri, D. T. Moir, M. S. Klempner, N. Krieger, G. Jones II, and L. D. Ziegler, J. Phys. Chem. B **109**, 312 (2005).
[20] R. M. Jarvis, A. Brooker, and R. Goodacre, Faraday Discuss. **132**, 281 (2006).
[21] L. Yeo, D. Hou, S. Maheshwari, and H.-C. Chang, Appl. Phys. Lett. **88**, 233512 (2006).
[22] R. Ohyama, K. Kaneko, and J.-S. Chang, IEEE Trans. Dielectr. Electr. Insul. **10**, 57 (2003).
[23] D. H. McCoy and M. M. Denn, Rheol. Acta **10**, 408 (1971).
[24] G. L. Leal, *Laminar Flow and Convective Transport Processes: Scaling Principles and Asymptotic Analysis* (Butterworth-Heinemann, 1992).
[25] L. Yeo, J. R. Friend, and D. R. Arifin, Appl. Phys. Lett. **89**, 103516 (2006); D. R. Arifin, L. Y. Yeo, and J. R. Friend, Biomicrofluidics **1**, 014103 (2007).
[26] P. C. Lee and D. Meisel, J. Phys. Chem. **86**, 3391 (1982).
[27] M. A. Young, D. A. Stuart, O. Lyandres, M. R. Glucksberg, and R. P. van Duyne, Can. J. Chem. **82**, 1435 (2004).